

Kazuhiro Watanabe

Quarkonium production at collider energies in Small- x formalism

Received: date / Accepted: date

Abstract I present a short review of recent studies of quarkonium production in proton-proton and proton-nucleus collisions at collider energies in Small- x formalism.

Keywords Quarkonium Production · Gluon Saturation · Proton-Nucleus Collision

1 Introduction

Quarkonium production in proton-proton (pp) collisions and proton-nucleus (pA) collisions at high scattering energies provide unique opportunities to investigate the so-called nonlinear gluon saturation [1; 2; 3] in hadron and heavy nucleus. The saturation scale Q_s^2 , which can be indeed expressed as $Q_{sA}^2 \sim A^{1/3} x^{-\lambda}$ where A is the atomic mass number and $\lambda \sim 0.3$, roughly separates nonlinear regime $Q^2 < Q_s^2$ from linear regime $Q^2 > Q_s^2$ with Q being a scale of external probe. At small Bjorken x , the saturation scale in a heavy nucleus becomes comparable with heavy quark mass and should characterize quarkonium production at low transverse momentum p_\perp in pA collisions. The gluon saturation is considered as Cold Nuclear Matter effect which has to be distinguished from hot medium effect in high energy heavy ion collisions [4].

Heavy quark pair production in pA collisions as a dilute-dense system, has been studied in the Color-Glass-Condensate (CGC) framework or Small- x saturation formalism in a general sense [5; 6; 7]. In the CGC framework, a rapid increase of gluon density inside hadron/nucleus at small- x is described in terms of JIMWLK equation [8; 9; 10; 11; 12] or Balitsky-Kovchegov (BK) equation [13; 14] which resums large logarithmic correction $\alpha_s \ln 1/x$.

On the other hand, elemental quarkonium production mechanism is not fully understood and depends on model or approach [15]. Specifically, three kinds of approaches have been employed for describing bound state formation in the Small- x formalism: i) Color Singlet Model (CSM) in which quarkonium is produced directly by emitting hard gluons. This gluon emission is required to make a heavy quark pair in color singlet state with right quantum numbers. ii) Color Evaporation Model (CEM) in which all of produced quark pairs with invariant mass below a threshold convert into quarkonium with a non-perturbative transition probability. iii) Non-Relativistic QCD (NRQCD) factorization based approach which is sophisticated to take into account both color octet and singlet quark pair according to velocity of heavy quark expansion. Indeed, each of the approaches yields different argument for quarkonium production in the Small- x formalism.

Invited presentation at the workshop "New Observables In Quarkonium Production", ECT*, Italy, 28 February - 4 March 2016.

K. Watanabe
Key Laboratory of Quark and Lepton Physics (MOE) and Institute of Particle Physics, Central China Normal University, Wuhan 430079, China
Present address: Physics Department, Old Dominion University, Norfolk, VA 23529, and Theory Center, Jefferson Lab, Newport News, VA 23606
E-mail: kazuhr.watanabe@gmail.com

Nowadays, the availability of an abundance of data accumulated by RHIC and LHC have enabled us to constrain the quarkonium production mechanism in the Small- x formalism and understand further the gluon dynamics in hadron and nucleus at small- x . The purpose of this paper is aimed at reviewing studies of quarkonium production in the Small- x formalism and clarifying issues in this respect. This paper is organized as follows: In Sec. 2, we start with an idea of effective factorization valid in forward quarkonium production in pA collisions which can help to understand building blocks for describing quarkonium production in the Small- x formalism. In Sec. 3, we review the CGC framework for describing heavy quark pair production in dilute-dense system, such as pA collision. Currently, the CGC framework available for heavy quark pair production is leading order (LO) in the strong coupling expansion with the quantum evolution of the wave function of target nucleus which is embodied by JIMWLK or BK equation. Some technical comments in this respect are given in Sec. 4. In Sec. 5, we classify quarkonium production models or approaches and then comparisons between the theoretical results for forward J/ψ production in the CGC framework with data of RHIC and LHC are displayed in Sec. 6. Finally, in Sec. 7, the importance of Sudakov factor for Υ production in the Small- x formalism is referred.

2 Quarkonium probing the gluon saturation

In this section, let us remind the reason why quarkonium production in pA collisions can be a valuable probe to the gluon saturation in target nucleus at high scattering energy. We first follow the discussion in Ref. [16] about a separation of relevant time scales in rest frame of target nucleus.

In rest frame of target nucleus at fixed target experiments, the interaction time when proton scatters off nucleus is characterized by $\tau_{int} \sim R_A$ in natural unit. Just after the pA collision, a heavy quark pair ($q\bar{q}$) is produced over the time $\tau_P \sim \frac{1}{2m_q} \frac{E_g}{2m_q}$ in the nucleus rest frame. Here m_q is quark mass and E_g is energy of parent gluon which subsequently splits into the $q\bar{q}$. Due to momentum conservation for partonic scattering process, $(2m_q)^2 = x_p x_A S_{NN} = 2x_p x_A M_N E_p$ with $x_{p,A}$ being longitudinal momentum fractions of projectile proton and target nucleus carried by incident gluons. M_N is mass of nucleon and $E_g = x_p E_p$. Then, one finds $\tau_P \sim \frac{1}{2x_A M_N}$. In this respect, at forward rapidity (proton going direction) in the high scattering energies, the $q\bar{q}$ production time τ_P is much longer than τ_{int} owing to Lorentz time dilation and the projectile proton interacts coherently with the whole nucleus. In other words, the $q\bar{q}$ pair is produced coherently in pA collision at high energy. Indeed, the coherent interaction between the $q\bar{q}$ and a large number of gluons in the target nucleus can reflect important information on the gluon saturation. The time scale of J/ψ formation can be estimated as $\tau_F \sim \frac{2}{M_{\psi'} - M_{J/\psi}} \frac{E_g}{M_{J/\psi}}$ with $M_{J/\psi}$ mass of J/ψ and $M_{\psi'}$ mass of ψ' . Since the binding energy of quarkonium is much smaller than m_q , one can find

$$\tau_F \gg \tau_P \gg \tau_{int}. \quad (1)$$

Then, bound state is formed enough outside of target nucleus at high scattering energies. In other words, dynamics of bound state formation can be decoupled with cold nuclear effects. Eq. (1) should be valid in the center of mass frame where $\tau_{int} \sim R_A/\gamma$ with γ the Lorentz factor.

Next, by following the discussion in Ref. [17], let us elaborate kinematical range in the center of mass system of pA collision where the factorization (1) is valid. Quarkonium production at low transverse momentum P_\perp should be characterized by the saturation scale, namely, $\Lambda_{QCD} \ll P_\perp \sim Q_{sA} \ll M$ with M quarkonium mass. In NRQCD and CEM actually [18], heavy quark velocity (v) is important parameter in addition to α_s for description of quarkonium production. If $Q_{sA} \sim m_q v \sim Mv/2$, multiple scattering of the $q\bar{q}$ in target nucleus can interfere with bound state formation, since Q_{sA} is short distance scale while $m_q v$ is long distance scale. Then, the v -expansion in the $q\bar{q}$ production amplitude, which is assumed to be true in NRQCD and CEM, is not clear. Nevertheless, in the very forward rapidity region, Lorentz time dilation leads to

$$\frac{1}{mv} \frac{P_\parallel}{M} \gg \frac{1}{P_\perp} \sim \frac{1}{Q_{sA}} \quad (2)$$

where $P_\parallel \approx M \cosh y$. As long as $y \gg \ln \frac{2mv}{P_\perp} \sim \ln \frac{Mv}{Q_{sA}}$, the scale in association with hadronization can be decouple with the short distance saturation scale. Then the bound state formation of the $q\bar{q}$ is effectively frozen when the $q\bar{q}$ passes through the target nucleus. The effective factorization between the $q\bar{q}$ coherent interaction in the target nucleus and the bound state formation is justified only at forward rapidity in both

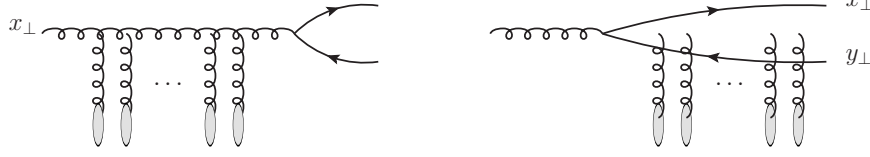


Fig. 1 Partonic scatterings at leading order for heavy quark pair production in pA collisions.

CEM and NRQCD approach. Thus, we can investigate the gluon saturation dynamics through quarkonium production in pA collisions.

3 Heavy quark pair production in dilute-dense system

In this section, we review that the $q\bar{q}$ production in pA collisions in the Small- x framework. Currently, the $q\bar{q}$ production cross section at leading order (LO) is only available. Blaizot-Gelis-Venugopalan derived the LO cross section for $q\bar{q}$ production in momentum space with the covariant gauge (the CGC framework, hereafter) [19; 20]. A similar formula for single quark production is derived by Tuchin but the derivation has been done in coordinate space with the light cone gauge [21]. Further, they independently discussed improvements by including quantum evolution correction embodied in the JIMWLK or the BK equation [22; 23]. In this paper, we restrict our attention to the CGC framework derived by Blaizot et al. because k_\perp -factorization approximation is manifest in this formula¹.

3.1 Framework

The CGC framework can provide a systematic description of the gluon saturation phenomena at high scattering energy. In the CGC framework, pA collision can be regarded as a collision of two classical fields moving along light cone axes. Here let us choose the light cone frame where projectile proton is going along light cone “+” axis while target nucleus is moving along light cone “-” direction. Valence partons at large- x are described by the solution of classical Yang-Mills equation [19]:

$$[D_\mu, F^{\mu\nu}] = J^\nu \quad (3)$$

with $J^\nu = g\delta^{\nu+}\delta(x^-)\rho_p(x_\perp) + g\delta^{\nu-}\delta(x^+)\rho_A(x_\perp)$ being the color current of pA collision. ρ_p and ρ_A are the color charge densities of valence parton in the proton and the nucleus, respectively. The background gauge field created in pA collision is $\mathcal{O}(\rho_p^1\rho_A^\infty)$. Meanwhile, gluons at small- x are produced from the large- x valence partons by the bremsstrahlung. The small- x gluon emissions can be described systematically in terms of the JIMWLK equation or the BK equation.

The $q\bar{q}$ production amplitude from the background gauge fields of $\mathcal{O}(\rho_p^1\rho_A^\infty)$ can be described as

$$M_{s_1 s_2; i j}(q, p) = \frac{g^2}{(2\pi)^4} \int d^2 k_\perp d^2 k_{1\perp} \frac{\rho_p(k_{1\perp})}{k_{1\perp}^2} \int d^2 x_\perp d^2 y_\perp e^{ik_\perp \cdot x_\perp} e^{i(P_\perp - k_\perp - k_{1\perp}) \cdot y_\perp} \\ \times \bar{u}_{s_1, i}(q) \left[T_g(k_{1\perp}) t^b W^{ba}(x_\perp) + T_{q\bar{q}}(k_{1\perp}, k_\perp) U(x_\perp) t^a U^\dagger(y_\perp) \right] v_{s_2, j}(p) \quad (4)$$

where

$$T_{q\bar{q}}(k_{1\perp}, k_\perp) \equiv \frac{\gamma^+(\not{q} - \not{k} + m) \gamma^-(\not{q} - \not{k} - \not{k}_1 + m) \gamma^+}{2p^+[(q_\perp - k_\perp)^2 + m^2] + 2q^+[(q_\perp - k_\perp - k_{1\perp})^2 + m^2]}, \\ T_g(k_{1\perp}) \equiv \frac{\not{C}_L(p + q, k_{1\perp})}{(p + q)^2}, \quad (5)$$

¹ Exactly speaking, k_\perp -factorization is violated for the $q\bar{q}$ production in pA collisions. See Refs. [23; 24]. k_\perp -factorization is ensured when the target nucleus is dilute system in which multiple scattering of the $q\bar{q}$ in the target nucleus is replaced by one gluon exchange.

where $C_L^\mu(p+q, k_{1\perp})$ is the Lipatov effective vertex and its components are defined as follows:

$$C_L^+(q, k_{1\perp}) \equiv \frac{-k_{1\perp}^2}{q^-} + q^+, \quad C_L^-(q, k_{1\perp}) \equiv \frac{k_{2\perp}^2}{q^+} - q^-, \quad C_L^i(q, k_{1\perp}) \equiv -2k_1^i + q^i. \quad (6)$$

u and v are spinors of quark and antiquark with spin s_1 and s_2 , respectively. q and p are three momentum of produced quark and antiquark, respectively. $k_{1\perp}$ is transverse momentum of incident gluon from projectile proton. $k_{2\perp} \equiv p_\perp + q_\perp - k_{1\perp}$ is net transverse momentum transfer from target nucleus. Eq. (4) contains two simple processes as depicted in Fig. 1: (i) an incident gluon from projectile proton suffers multiple scatterings with a large number of gluons in target nucleus and subsequently the gluon splits into a $q\bar{q}$ pair. (ii) a $q\bar{q}$ pair is produced from the incident gluon which scatters off the target nucleus. Therefore the $q\bar{q}$ pair is produced coherently in pA collisions.

At high scattering energies, transverse positions of quark and gluon are almost frozen during the multiple scattering process. This fact ensures the use of Eikonal approximation. The interaction between incident quark (gluon) and the dense gluons in the target nucleus can be expressed as the Wilson line in the fundamental (adjoint) representation:

$$U(x_\perp) = \mathcal{P}_+ \exp \left[ig \int_{-\infty}^{+\infty} dz^+ A_A^-(z^+, x_\perp) \cdot t \right], \\ W(x_\perp) = \mathcal{P}_+ \exp \left[ig \int_{-\infty}^{+\infty} dz^+ A_A^-(z^+, x_\perp) \cdot T \right] \quad (7)$$

where $A^-(z^+, x_\perp)$ is the background gauge field of the target nucleus and related to ρ_A . t^a and T_{ij}^a are the generators of the fundamental and adjoint representations of SU(3) group, respectively.

In order to convert the $q\bar{q}$ production amplitude into the $q\bar{q}$ production cross section at classical level, it is required to average the squared amplitude over the distributions of the classical color sources ρ_p and ρ_A as follows:

$$\frac{d\hat{\sigma}_{q\bar{q}}}{d^2q_\perp d^2p_\perp dy_q dy_p} = \frac{1}{[2(2\pi)^3]^2} \int d^2b_\perp \int \mathcal{D}\rho_p \mathcal{D}\rho_A W_p[\rho_p] W_A[\rho_A] |M_{s_1 s_2; ij}(q, p)|^2 \quad (8)$$

where W_p and W_A are the weight functionals of ρ_p and ρ_A . The $q\bar{q}$ is produced at impact parameter b_\perp in pA collision. Rapidity dependence of Eq. (8) is embodied in the weight functionals which obey the JIMWLK equation [7].

3.2 Multi-point Wilson line correlators

Multi-point Wilson line correlators, which appear in Eq. (8) constitute wave function of target nucleus in the high energy region. In fact, Multi-point Wilson line correlator can be determined uniquely by color state of produced $q\bar{q}$. It is well known that color and spin of produced $q\bar{q}$ are significant ingredients for describing quarkonium production in CSM, CEM, and NRQCD factorization which are more explained in Sec. 5. Then, let us clarify Multi-point Wilson line correlators according to colors of produced $q\bar{q}$ in pA collision.

3.2.1 Summed up all of the color states

We first consider that all of the spin and color of produced $q\bar{q}$ is summed up. This case leads to quarkonium production in CEM. By summing up the spin and the color of $q\bar{q}$, Eq. (8) can be cast into

$$\frac{d\sigma_{q\bar{q}}}{d^2q_\perp d^2p_\perp dy_q dy_p} = \frac{\alpha_s}{(2\pi)^6 C_F} \int \frac{d^2k_{1\perp}}{(2\pi)^2} \frac{\Phi_{p, Y_p}(k_{1\perp})}{k_{1\perp}^2 k_{2\perp}^2} \\ \times \underbrace{\left[\int \frac{d^2k_\perp d^2k'_\perp}{(2\pi)^4} \Xi^{q\bar{q}, q\bar{q}} \phi_{A, Y_A}^{q\bar{q}, q\bar{q}} + \int \frac{d^2k_\perp}{(2\pi)^2} \Xi^{q\bar{q}, g} \phi_{A, Y_A}^{q\bar{q}, g} + \Xi^{g, g} \phi_{A, Y_A}^{g, g} \right]}_{\Rightarrow \int \frac{d^2k_\perp}{(2\pi)^2} \Xi(k_{1\perp}, k_{2\perp}, k_\perp) \phi_{A, Y_A}^{q\bar{q}, g}(k_{2\perp}, k_\perp)} \quad (9)$$

where the large- N_c approximation and the sum rule² have been used. $\Xi = \Xi^{q\bar{q},q\bar{q}} + \Xi^{q\bar{q},g} + \Xi^{g,g}$ is the partonic hard scattering part. $\varphi_{p,x}(k_\perp)$ is the unintegrated gluon distribution function (UGDF) of projectile proton³ and its definition is given by

$$\varphi_{p,Y_p}(k_\perp) = \frac{(2\pi)^2 \alpha_s S_\perp}{k_\perp^2} \int d^2 x_\perp e^{ik_\perp \cdot x_\perp} \langle \rho_p(0) \rho_p(x_\perp) \rangle_{Y_p}. \quad (10)$$

The multi-point Wilson line correlator of the target nucleus in the large- N_c limit can be written as

$$\begin{aligned} \phi_{A,Y_A}^{q\bar{q},g}(k_{2\perp}, k_\perp) &\equiv S_\perp \frac{N_c k_{2\perp}^2}{2} \int d^2 x_\perp d^2 y_\perp e^{ik_\perp \cdot x_\perp + i(k_{2\perp} - k_\perp) \cdot y_\perp} \frac{1}{N_c^2} \langle \text{tr}[U(x_\perp) t^a U^\dagger(y_\perp) t^b W_{ba}(0_\perp)] \rangle_{Y_A} \\ &\approx S_\perp \frac{N_c k_{2\perp}^2}{4} F_{Y_A}(k_{2\perp} - k_\perp) F_{Y_A}(k_\perp) \end{aligned} \quad (11)$$

where the Fierz identity and the identity $t^b W^{ba}(x_\perp) = U(x_\perp) t^a U^\dagger(x_\perp)$ have been used. Fourier transform of the fundamental dipole amplitude is defined as

$$F_Y(k_\perp) \equiv \int d^2 x_\perp e^{-ik_\perp \cdot x_\perp} S_Y(x_\perp) = \int d^2 x_\perp e^{-ik_\perp \cdot x_\perp} \frac{1}{N_c} \langle \text{Tr}[U(x_\perp) U^\dagger(0_\perp)] \rangle_Y. \quad (12)$$

The subscript $Y_{p,A} = \ln 1/x_{p,A}$ of $\langle \dots \rangle$ above represents the rapidity gap between the $q\bar{q}$ and the projectile proton or the target nucleus. $x_p = k^+/P_p^+$ and $x_A = k^-/P_A^-$ are the longitudinal momentum fraction of the projectile proton and the target nucleus carried by the incident gluon, respectively. By assuming the impact parameter dependence in pA collision is weak, transverse size of nucleus S_\perp is appeared explicitly. This assumption is essential to manage the CGC framework.

3.2.2 Colorless and Colored intermediate states

In order to employ CSM and NRQCD approach, the use of NRQCD projection operators associated with spin, angular momentum, and color of $q\bar{q}$ is common but useful technique in this respect. As examined in Ref. [26], by using NRQCD projection operators, Eq. (4) can be cast into

$$\begin{aligned} M^{J_z, (1,8c)}(P) &= g^2 \int \frac{d^2 k_\perp d^2 k_{1\perp}}{(2\pi)^4} \frac{\rho_p(k_{1\perp})}{k_{1\perp}^2} \int d^2 x_\perp d^2 y_\perp e^{ik_\perp \cdot x_\perp} e^{i(P_\perp - k_\perp - k_{1\perp}) \cdot y_\perp} \\ &\times \left\{ \text{tr}[C^{(1,8c)} t^b W^{ba}(x_\perp)] \mathcal{F}_g^{J_z}(P, k_{1\perp}) + \text{tr}[C^{(1,8c)} U(x_\perp) t^a U^\dagger(y_\perp)] \mathcal{F}_{q\bar{q}}^{J_z}(P, k_{1\perp}, k_\perp) \right\} \end{aligned} \quad (13)$$

where

$$\mathcal{F}_{q\bar{q}}^{J_z}(P, k_{1\perp}, k_\perp) = \sum_{L_z, S_z} \langle LL_z; SS_z | JJ_z \rangle \times \begin{cases} \text{tr}[\Pi^{S, S_z} T_{q\bar{q}}(g)]|_{q=0} & (\text{S-wave}) \\ \varepsilon_\mu^*(L_z) \frac{\partial}{\partial q^\mu} \text{tr}[\Pi^{S, S_z} T_{q\bar{q}}(g)]|_{q=0} & (\text{P-wave}) \end{cases} \quad (14)$$

where $P(q)$ is total (relative) momentum of $q\bar{q}$ pair. $\varepsilon_\mu^*(L_z)$ is polarization vector of produced $q\bar{q}$ with angular momentum L_z . By following Ref. [26], the color projection operators are defined as $C^1 = 1/\sqrt{N_c}$ and $C^{8c} = \sqrt{2}t^c$ [26] and the covariant spin projection operators are defined as

$$\Pi^{S, S_z} = \sqrt{\frac{1}{m}} \sum_{s_1, s_2} \left\langle \frac{1}{2}, s_1; \frac{1}{2}, s_2 \middle| S, S_z \right\rangle v(p) \bar{u}(q) \quad (15)$$

where $\sqrt{\frac{1}{m}}$ is the normalization factor⁴. It is straightforward to obtain differential cross section for single $q\bar{q}$ production in specific intermediate states, as shown in Eq. (8). However, the full formula for the $q\bar{q}$ production

² In general, $\int \frac{d^2 k_\perp d^2 k'_\perp}{(2\pi)^4} \phi_{A,Y_A}^{q\bar{q},q\bar{q}} = \int \frac{d^2 k_\perp}{(2\pi)^2} \phi_{A,Y_A}^{q\bar{q},g} = \phi_{A,Y_A}^{g,g}$.

³ $\phi_{p,x}^{g,g}$ is reduced to $\varphi_{p,x}$ at leading twist by definition. Indeed, $\phi_{p,x}^{g,g}$ is mostly used instead of $\varphi_{p,x}$ in numerical calculations because it is easy to take into account quantum evolution effect for projectile proton [25].

⁴ $\bar{u}u = -\bar{v}v = 2m$ for free Dirac spinors and $\langle q\bar{q}|q\bar{q} \rangle = 4m$ for composite field yield the normalization factor $\frac{\sqrt{4m}}{\sqrt{2m}\sqrt{2m}} = \sqrt{\frac{1}{m}}$.

with the NRQCD projection operators are complicated⁵. Then, let us pick up some essential points for understanding the CGC framework with NRQCD factorization.

For the $q\bar{q}$ production in color singlet intermediate state, it is required to replace the partonic hard scattering part and the wave function of the target nucleus by

$$\begin{aligned} \frac{d\sigma_{q\bar{q}}^{\text{CS}}}{d^2P_\perp dy} &= \frac{2\alpha_s}{(2\pi)^3(N_c^2 - 1)} \int \frac{d^2k_{1\perp} d^2k_\perp d^2k'_\perp}{(2\pi)^6} \frac{\phi_{p,Y_p}(k_{1\perp})}{k_{1\perp}^2} \frac{1}{2J+1} \sum_{J_z} \mathcal{F}_{q\bar{q}}^{J_z}(P, k_{1\perp}, k_\perp) \mathcal{F}_{q\bar{q}}^{J_z^\dagger}(P, k_{1\perp}, k'_\perp) \\ &\times \int d^2x_\perp d^2x'_\perp d^2y_\perp d^2y'_\perp e^{i(k_{1\perp} \cdot x_\perp - k'_\perp \cdot x'_\perp)} e^{i(k_{2\perp} - k_\perp) \cdot y_\perp} e^{-i(k_{2\perp} - k'_\perp) \cdot y'_\perp} \frac{1}{N_c} \langle \text{tr}[U(x_\perp) t^a U^\dagger(y_\perp)] \text{tr}[U(y'_\perp) t^a U^\dagger(x'_\perp)] \rangle_{Y_A}. \end{aligned} \quad (16)$$

One understands immediately that the diagrams in Fig. 1 (left) never contribute to Eq. (16) because an incoming gluon, which is a colored object, never convert into a colorless object. Furthermore, with the use of the Fierz identity at the last line in Eq. (16), the multipoint Wilson line correlator can be cast into

$$\frac{1}{N_c} \langle \text{tr}[U(x_\perp) t^a U^\dagger(y_\perp)] \text{tr}[U(y'_\perp) t^a U^\dagger(x'_\perp)] \rangle_{Y_A} \approx \frac{1}{2} [Q_{Y_A}(x_\perp, y_\perp; y'_\perp, x'_\perp) - S_{Y_A}(x_\perp, y_\perp) S_{Y_A}(y'_\perp, x'_\perp)] \quad (17)$$

where the large- N_c approximation has been used. The first term in Eq. (17) is referred to as the quadrupole amplitude

$$Q_{Y_A}(x_\perp, y_\perp; y'_\perp, x'_\perp) \equiv \frac{1}{N_c} \text{tr} \langle U(x_\perp) U^\dagger(x'_\perp) U(y'_\perp) U^\dagger(y_\perp) \rangle_{Y_A}. \quad (18)$$

Interestingly, the quadrupole amplitude can survive even if the large- N_c limit is taken. This is a unique point that produced $q\bar{q}$ in color singlet intermediate state is capable of probing the quadrupole amplitude which is never appeared in Eq. (9). Here, if the impact parameter dependence is neglected, the transverse area S_\perp appears explicitly in Eq. (16).

Similarly, for the $q\bar{q}$ production in the color octet state, one finds

$$\begin{aligned} \frac{d\sigma_{q\bar{q}}^{\text{CO}}}{d^2P_\perp dy} &= \frac{2\alpha_s}{(2\pi)^3(N_c^2 - 1)} \int \frac{d^2k_{1\perp} d^2k_\perp d^2k'_\perp}{(2\pi)^6} \frac{\phi_{p,Y_p}(k_{1\perp})}{k_{1\perp}^2} \\ &\times \int d^2x_\perp d^2y_\perp d^2x'_\perp d^2y'_\perp e^{ik_{1\perp} \cdot x_\perp - ik'_\perp \cdot x'_\perp} e^{i(P_\perp - k_\perp - k_{1\perp}) \cdot y_\perp} e^{-i(P_\perp - k'_\perp - k_{1\perp}) \cdot y'_\perp} \\ &\times [\Xi_1^{\text{CO}} \mathcal{W}_{Y_A}(x, y; y', x') + \Xi_2^{\text{CO}} \mathcal{W}_{Y_A}(x, y; x', x') + \Xi_3^{\text{CO}} \mathcal{W}_{Y_A}(x, x; y', x') + \Xi_4^{\text{CO}} \mathcal{W}_{Y_A}(x, x; x', x')] \end{aligned} \quad (19)$$

where $\Xi_{1\sim 4}^{\text{CO}}$ are the hard matrix elements and

$$\begin{aligned} \mathcal{W}_{Y_A}(x, y; y', x') &\equiv \frac{2}{N_c^2 - 1} \langle \text{tr}[t^c U(x_\perp) t^a U^\dagger(y_\perp)] \text{tr}[U(y'_\perp) t^a U^\dagger(x'_\perp) t^c] \rangle_{Y_A} \\ &= \frac{1}{2(N_c^2 - 1)} \left[\langle \text{tr}[U(y'_\perp) U^\dagger(y_\perp)] \text{tr}[U(x_\perp) U^\dagger(x'_\perp)] \rangle_{Y_A} - \frac{1}{N_c} \langle \text{tr}[U(x_\perp) U^\dagger(y_\perp) U(y'_\perp) U^\dagger(x'_\perp)] \rangle_{Y_A} \right. \\ &\quad \left. - \frac{1}{N_c} \langle \text{tr}[U(x_\perp) U^\dagger(x'_\perp) U(y'_\perp) U^\dagger(y_\perp)] \rangle_{Y_A} + \frac{1}{N_c^2} \langle \text{tr}[U(x_\perp) U^\dagger(y_\perp)] \text{tr}[U(y'_\perp) U^\dagger(x'_\perp)] \rangle_{Y_A} \right] \\ &\approx \frac{1}{2} S_{Y_A}(y'_\perp, y_\perp) S_{Y_A}(x_\perp, x'_\perp). \end{aligned} \quad (20)$$

The last line in Eq. (20) is manifest in the large- N_c approximation. The large- N_c approximation further reduces Eq. (19) to

$$\frac{d\sigma_{q\bar{q}}^{\text{CO}}}{d^2P_\perp dy} = \frac{\alpha_s S_\perp}{(2\pi)^3(N_c^2 - 1)} \int \frac{d^2k_{1\perp} d^2k_\perp}{(2\pi)^4} \frac{\phi_{p,Y_p}(k_{1\perp})}{k_{1\perp}^2} F_{Y_A}(k_{2\perp} - k_\perp) F_{Y_A}(k_\perp) \Xi^{\text{CO}} \quad (21)$$

with $\Xi^{\text{CO}} = \sum_i \Xi_i^{\text{CO}} = \frac{1}{2J+1} \sum_{J_z} |\mathcal{F}_{q\bar{q}}^{J_z} + \mathcal{F}_g^{J_z}|^2$. This formula is the same as Eq. (9) to the extent that the multipoint Wilson line correlators can be represented by means of the dipole amplitude only, although the hard matrix elements are different. Of particular importance is that the nuclear effect is the same both in CEM and the color octet state in NRQCD with the large- N_c approximation [17; 26].

⁵ For the detailed calculations, see Ref. [26].

3.3 Forward production : Hybrid approach

At forward rapidity ⁶ where $x_p \sim 1$, the phase space of the gluon distribution in projectile proton shrinks. As discussed in [23; 25; 26], it is not hard to realize that all of the hard matrix elements in Eqs. (9)(16)(21) are quadratic in $k_{1\perp}$ when $k_{1\perp} \rightarrow 0$. This fact justifies taking the limit $k_{1\perp} \rightarrow 0$ in the hard scattering parts and replacing the unintegrated gluon distribution function with the collinear gluon distribution function (PDF), although the multi-point Wilson line correlator constitutes the wave function of the target nucleus. This asymmetric treatment at $x_p \sim 1$ and $x_A \ll 1$ is referred to as Hybrid formalism. The UGDF is related to the usual collinear gluon PDF with the following definition:

$$x_p G(x_p, \mu) \equiv C \int^{\mu^2} dk_{\perp}^2 \phi_{p,Y_p}(k_{\perp}) \quad (22)$$

with C being the normalization factor ⁷.

4 Quantum evolution at small- x

For phenomenological studies, the dipole amplitude is particularly important to take into account the quantum evolution effect at small- x easily. In this section, a couple of approaches to describe the rapidity dependence of the dipole amplitude, which are used in recent studies on quarkonium production in the Small- x formalism, are presented. Some comments about the quadrupole amplitude are also presented.

4.1 The dipole amplitude

In GBW model [27], the dipole amplitude can be written as

$$S_Y(r_{\perp}) = \exp \left[-\frac{Q_s^2 r_{\perp}^2}{4} \right] \quad (23)$$

where the saturation scale is assumed to be $Q_s^2(x) = A^{1/3} Q_{s0}^2 (x_0/x)^{\lambda}$ with $x_0 = 0.000304$, $\lambda = 0.288$ and c is constant. In GBW model, the rapidity dependence of the dipole amplitude is controlled by changing the saturation scale. GBW model is useful to enable us to take into account the saturation effect. Meanwhile, GBW model is not realistic model to the extent that GBW model can not describe the power of the UGDF at large k_{\perp} because of its exponential form.

Indeed, the dipole amplitude should obey BK equation which is defined as

$$-\frac{dS_Y(r_{\perp})}{dY} = \int d^2 r_{1\perp} \mathcal{K}(r_{\perp}, r_{1\perp}) [S_Y(r_{\perp}) - S_Y(r_{1\perp}) S_Y(r_{2\perp})] \quad (24)$$

with $\mathbf{r}_{\perp} = \mathbf{r}_{1\perp} + \mathbf{r}_{2\perp}$. The rapidity dependence of the dipole amplitude can be completely determined by the evolution kernel \mathcal{K} and the initial condition. At present, BK equation with running coupling effect (rcBK equation) [28] is the state of the art technology to describe appropriately the speed of the quantum evolution and employed in many phenomenological studies [25; 29; 30; 31].

The initial condition of the rcBK equation for proton can be constrained by global data fitting at HERA DIS ⁸. As is performed in Refs. [32; 33; 34], in order to constrain the rcBK initial condition, the modified McLerran-Venugopalan (MV) model [35] is used at $x_0 = 0.01$ with the following functional form:

$$S_{x=x_0}(r_{\perp}) = \exp \left[-\frac{(r_{\perp}^2 Q_{s0}^2)^{\gamma}}{4} \ln \left(\frac{1}{|r_{\perp}| \Lambda} + e_c \cdot e \right) \right]. \quad (25)$$

Currently, there are normally two kinds of the parameters sets available for the initial condition of the rcBK equation: (i) the parameters set referred to as MV^{γ} where $\gamma \neq 1$ and $e_c = 1$ [32; 33]. (ii) the so-called MV^e

⁶ In this paper, proton moving direction (nucleus moving direction) is defined as forward (backward).

⁷ As an example, $C = \frac{1}{4\pi^3}$ is chosen in Ref. [23].

⁸ In fact, it is also required to constrain not only the dipole amplitude but also the one-loop coupling constant in the coordinate space simultaneously. See [32; 33; 34].

set where $\gamma = 1$ and $e_c \neq 1$ [34]. Naturally, all of the other relevant parameters are different between MV^γ and MV^e . Both MV^γ and MV^e provide quite similar behaviors of the dipole amplitude when x is small. When $\gamma = 1$ and $e_c = 1$, Eq. (25) recovers the quasi-classical MV model which resums multiple scattering effect of $q\bar{q}$ in target nucleus as well as GBW model.

In contrast to the initial condition for proton, we need to set a model for initial condition of the rcBK equation for nucleus owing to lack of precise data of $e + A$ collision, although a future Electron Ion Collider (EIC) experiment can constrain the initial condition of the rcBK equation for nucleus. In fact, the following model approaches have been studied.

- *Homogeneous approximation*

The saturation scale for nucleus should be proportional to atomic mass number A by the definition. If the impact parameter dependence is weak in pA collision and the saturation scale does not change rapidly in transverse plane of nucleus, the saturation scale for nucleus at $x = x_0$ in Eq. (25) can be replaced as

$$Q_{s0,A}^2 = N_{\text{coll}} Q_{s0}^2 \approx cA^{1/3} Q_{s0}^2. \quad (26)$$

Then, the information of target nucleus is reflected only in the saturation scale except for transverse are of nucleus. Eq. (26) is reasonable approximation as long as we restrict our attention to minimum bias events in pA collisions [25; 36; 37]. Although $c = 1$ is naively expected, $c \sim 0.5$ is indeed suggested for minimum bias events from nuclear DIS analysis performed in Ref. [38].

- *Glauber model approach*

In Refs. [34; 39; 40], more realistic treatment for nuclear dependence is considered by employing optical-Glauber model in the rcBK initial condition with MV^e parametrization as follows:

$$S_{x=x_0}(r_\perp; b_\perp) = \exp \left[-AT_A(b_\perp) \frac{\sigma_0}{2} \frac{r_\perp^2 Q_{s0}^2}{4} \ln \left(\frac{1}{|r_\perp| \Lambda} + e_c \cdot e \right) \right] \quad (27)$$

where $T_A(b_\perp)$ is the Woods-Saxon nucleon distribution in nucleus. $\frac{\sigma_0}{2} = \int d^2b_\perp$ is the effective transverse area of proton⁹ which is determined by fitting of HEAR DIS data [34]. This treatment enables us to compute event activity dependence of quarkonium production in pA collisions.

4.2 Quadrupole amplitude

The quadrupole amplitude is necessary to compute the $q\bar{q}$ pair production in the color singlet intermediate state as mentioned in the previous section. In principle, the JIMWLK equation controls the rapidity dependence of the quadrupole amplitude. However, it is complicated to solve the JIMWLK equation numerically. Interestingly, if the distribution of the color charge density in nucleus is the Gaussian form, the quadrupole amplitude can reduce to the following expression analytically [20; 41]:

$$Q_Y(x_\perp, y_\perp; y'_\perp, x'_\perp) \approx S_Y(x_\perp, x'_\perp) S_Y(y'_\perp, y_\perp) - \frac{\ln [S_Y(x_\perp, y'_\perp) S_Y(x'_\perp, y_\perp)] - \ln [S_Y(x_\perp, y_\perp) S_Y(x'_\perp, y'_\perp)]}{\ln [S_Y(x_\perp, x'_\perp) S_Y(y'_\perp, y_\perp)] - \ln [S_Y(x_\perp, y_\perp) S_Y(x'_\perp, y'_\perp)]} \times [S_Y(x_\perp, x'_\perp) S_Y(y'_\perp, y_\perp) - S_Y(x_\perp, y_\perp) S_Y(x'_\perp, y'_\perp)] \quad (28)$$

where the large- N_c approximation has been assumed. Then, the rapidity evolution of the quadrupole amplitude can be achieved through the dipole amplitude.

5 Bound state formation

Description of nonperturbative bound state formation at long distance is obviously a challenge for quarkonium production in the Small- x formalism. There is no rigorous proof of factorization between the $q\bar{q}$ production and the bound state formation in the CGC framework. Nevertheless, as mentioned in Sec. 2, it is supposed that the $q\bar{q}$ production never interfere in the bound state formation, since the produced $q\bar{q}$ is going to be bound sufficiently outside of the target nucleus at forward rapidity in the high energy region. Thus far, quarkonium production in the CGC framework have been studied by employing CSM, CEM, and NRQCD factorization.

⁹ Roughly speaking, Projectile proton beam with a transverse size $\frac{\sigma_0}{2}$ picks up nucleons in target nucleus.

5.1 Color Evaporation Model

Color Evaporation Model (CEM) is simple phenomenological approach and manageable to perform numerical calculations. The CEM has been used in Refs. [23; 25; 37; 39; 40]. In the CEM, the invariant mass of the $q\bar{q}$ pair is integrated from the bare $q\bar{q}$ mass ($2m_q$) to the threshold of decay into an open heavy flavor meson pair ($2M_h$) as follows:

$$\frac{d\sigma_\psi}{d^2P_\perp dY} = F_{q\bar{q} \rightarrow \psi} \int_{(2m_q)^2}^{(2M_h)^2} dM^2 \frac{d\sigma_{q\bar{q}}}{dM^2 d^2P_\perp dY}. \quad (29)$$

The produced $q\bar{q}$ pair is going to be bound into a quarkonium ψ with the probability $F_{q\bar{q} \rightarrow \psi}$. $F_{q\bar{q} \rightarrow \psi}$ is universal empirical factor which should be interpreted as a normalization factor for inclusive ψ production. Furthermore, one must keep in mind that any K -factor in association with higher order correction is included in $F_{q\bar{q} \rightarrow \psi}$ as well. The $q\bar{q}$ production cross section is calculated by summing up all of the color and the spin of $q\bar{q}$ in final state.

5.2 Non-Relativistic QCD

Non-Relativistic QCD (NRQCD) factorization approach provides more sophisticated treatment for describing bound state formation. In the context of the CGC framework, NRQCD approach is employed in Refs. [26; 36; 31]. As discussed in Sec. 2, the quark velocity v -expansion in NRQCD is effectively ensured at forward rapidity and the ψ production can be written as:

$$\frac{d\sigma_\psi}{d^2P_\perp dY} = \sum_{\kappa} \frac{d\hat{\sigma}^\kappa}{d^2P_\perp dY} \langle \mathcal{O}_\psi^\kappa \rangle \quad (30)$$

where $d\hat{\sigma}^\kappa$ is differential cross section for $q\bar{q}$ production in quantum state κ . $\langle \mathcal{O}_\psi^\kappa \rangle$ is referred to as universal NRQCD long distance matrix elements (LDMEs) which is a probability to convert $q\bar{q}$ into ψ . LDMEs for color octet channel can be extracted from data by employing NRQCD with the collinear factorization framework at NLO [42; 43; 44]. Meanwhile, LDME for color singlet channel is provided by nonrelativistic wave function of $q\bar{q}$ at origin ($v=0$). In terms of NRQCD power counting, the important intermediate states for J/ψ or Υ production can be listed up to $\mathcal{O}(v^4)$ below:

$$^3S_1^{[1]}, \quad ^1S_0^{[8]}, \quad ^3S_1^{[8]}, \quad ^3P_0^{[8]} \quad (31)$$

where standard spectroscopic notation $^{2S+1}L_J^{[c]}$ is used. S is spin, L is angular momentum, J is total angular momentum, and c is color state of $q\bar{q}$. For J/ψ production from the $q\bar{q}$ in $^3S_1^{[1]}$, Eq. (16) is used as the partonic cross section. Meanwhile, Eq. (19) is used for J/ψ production from the $q\bar{q}$ in the other three channels.

5.3 Color Singlet Model

NRQCD factorization framework coincides with Color Singlet Model (CSM) by taking the limit $v \rightarrow 0$. In the context of the small- x physics, the CSM is employed in [16; 45; 46; 47; 48; 49; 50]. Interestingly, as indicated in Ref. [26], the color singlet channel in the CGC+NRQCD framework corresponds to quarkonium production in the CSM which is discussed in [48; 49], by setting a Gaussian form for the dipole amplitude like GBW model in Eq. (28).

It is well known that the color singlet channel does not give the dominant contribution for quarkonium production in pp collisions at larger P_\perp . However, as indicated in [16; 50], quarkonium production mechanism in pA collisions can be different from that in pp collisions, especially, in the lower P_\perp region.

Let us consider J/ψ production as an example. J/ψ has $J^{PC} = 1^{--}$ as the spin-parity-charge number. In order to satisfy this property, odd numbers of gluons are required in elementary partonic scattering. By assuming proton is a dilute object, the relevant partonic scattering process at leading order in pp collision is two gluon fusion as $g + g \rightarrow J/\psi + g$ where a soft gluon is radiated. The cross section of this process

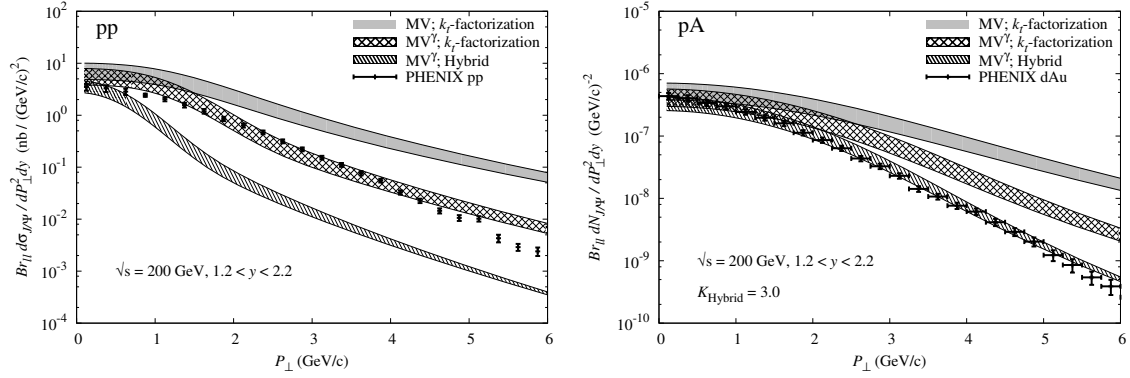


Fig. 2 Differential cross section as a function of P_\perp for J/ψ production in pp (left) and pA (right) collisions at RHIC at forward rapidity in the CGC+CEM framework. All of the input parameters are the same as used in Ref. [25]. Regarding the Hybrid formula in pA collision, K -factor of 3 is multiplied further to tune with data.

is $\mathcal{O}(\alpha_s^4)$ except for the gluon distribution function of the projectile proton¹⁰. On the other hand, for pA collisions, three gluons fusion process as $g + g + g \rightarrow J/\psi$ can be happened due to the multiple scattering of the $q\bar{q}$ in the target nucleus. The cross section of this process is $\mathcal{O}(\alpha_s^5 A^{2/3})$. Then, the three gluon fusion process seems to be suppressed compared to the two gluon fusion in terms of strong coupling. Nevertheless, the quasi-classical approximation $\alpha_s^2 A^{1/3} \sim \mathcal{O}(1)$ leads to $\mathcal{O}(\alpha_s^5 A^{2/3}) \rightarrow \mathcal{O}(\alpha_s)$. Therefore, the color singlet direct J/ψ production can be enhanced in pA collisions compared to pp collisions.

6 J/ψ production in the CGC vs Exp. data

We revisit the numerical results of J/ψ production in the CGC framework. In fact, $x_{p,A}$ can be determined from observables in final state by the relation $x_{p,A} = e^{\pm y} \sqrt{M^2 + P_\perp^2} / \sqrt{s}$. For J/ψ production, $10^{-2} \lesssim x_A \lesssim 10^{-3}$ at forward rapidity in the RHIC energy, while the LHC energy enable us to reach $10^{-4} \lesssim x_A \lesssim 10^{-5}$ at forward rapidity. Regarding the mid rapidity region at RHIC, $x_{p,A}$ are larger than x_0 . Then, it is expected that the onset of the gluon saturation is never appeared at RHIC at mid rapidity. Then, in this section, we restrict our attention into forward quarkonium production in pp and pA collisions in the RHIC and the LHC energies.

6.1 P_\perp -spectrums

Fig. 2 (left) shows the differential cross section as a function of P_\perp for J/ψ production in pp collision at RHIC at forward rapidity. The theoretical results are computed in the k_\perp -factorization formula and also the Hybrid formula within the CGC+CEM framework [25]. It is manifest that the P_\perp -spectrum strongly reflects the rcBK initial condition, since the RHIC kinematics enable us to investigate moderate small values of x_A in the vicinity of $x_0 = 0.01$.

The results of J/ψ production for minimum bias events in pA collisions in the CGC+CEM framework are also shown in Fig. 2 (right). The results are obtained by using Eq. (26) with $c = 1$ fixed. Due to the large saturation scale for nucleus, the P_\perp -spectrums are seemingly in good agreement with data, although the uncertainties associated with the initial condition of the rcBK equation and the framework itself (k_\perp -factorization or Hybrid formalism) are still large.

The results at LHC, which are shown in Fig. 3, indicate that the uncertainty associated with the initial condition of the rcBK equation becomes smaller due to the quantum evolution at lower P_\perp but the CGC+CEM framework fails to reproduce the data at high P_\perp where the CGC framework does not work any longer.

¹⁰ This power counting can be estimated as follows: In pp collision, the splitting $g \rightarrow q\bar{q}$ is $\mathcal{O}(\alpha_s)$, the gluon radiation is $\mathcal{O}(\alpha_s)$, the gluon exchange between q or \bar{q} and target proton provides $\mathcal{O}(\alpha_s^2)$. Then, the contribution in pp collision is $\mathcal{O}(\alpha_s^4)$ in total. In pA collision, the multiple gluon exchange between q or \bar{q} and target nucleus provides $\mathcal{O}(\alpha_s^2 A^{1/3})$. Then, one finds the contribution in pA collision is $\mathcal{O}(\alpha_s^5 A^{2/3})$ in total. Although this counting rule is slightly different from the original papers [16; 50], the idea is essentially the same.

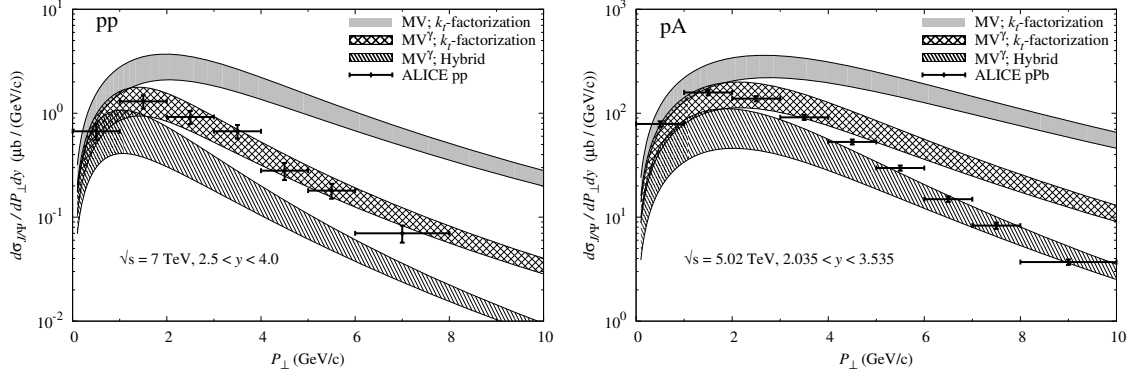


Fig. 3 P_{\perp} distribution of J/ψ production at LHC in the CGC+CEM framework. All of the input parameters are the same as used in Ref. [25]. Regarding pA collisions, the further normalization factor of 2 is multiplied.

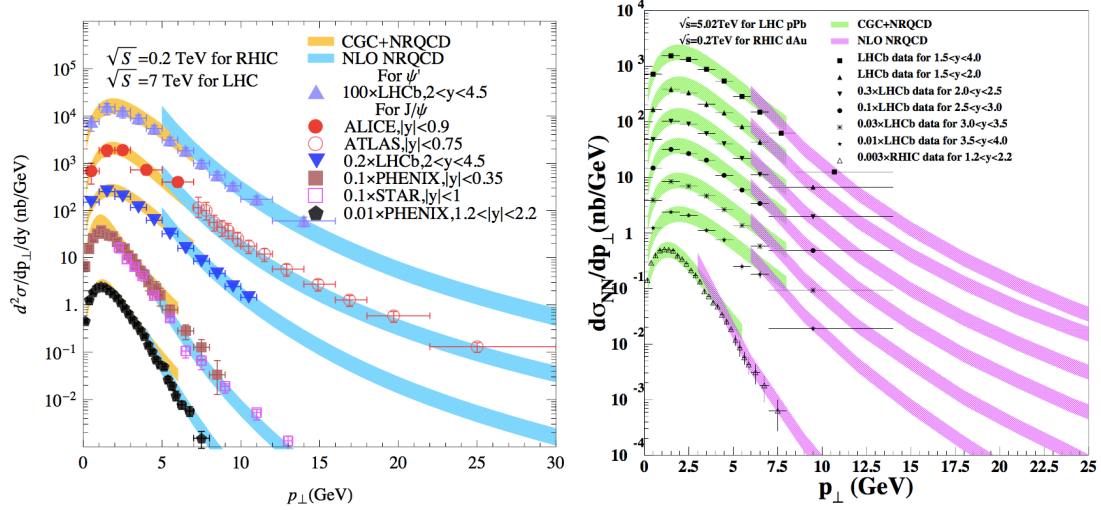


Fig. 4 P_{\perp} -spectrums of J/ψ production in pp (left) and pA (right) collisions in the CGC+NRQCD framework. The figures are taken from Refs. [31; 36].

A caution concerning the UGDF of the projectile proton at $x_p \geq x_0$ is noted here. The UGDF of the projectile proton used in the k_{\perp} -factorization framework does not necessarily correspond to the collinear gluon distribution function such as CTEQ PDF [51], even though Eq. (22) defines the relation between the UGDF and the collinear gluon PDF. In fact, extrapolation of the UGDF at x_0 is required at larger- x . For example, the phenomenological ansatz is employed in [23; 25; 37], while a matching approach between the UGDF and the collinear gluon distribution function numerically has been considered in Ref. [31]. In any case, one must keep in mind that the extrapolation of the UGDF at $x \geq x_0$ necessarily contains large systematic uncertainties.

Next, let us move into results of the CGC framework with the NRQCD factorization (CGC+NRQCD). Fig. 4 (left) shows the numerical results for J/ψ production (and also ψ' for comparison) in pp collisions in the CGC+NRQCD at RHIC and LHC. These calculations are performed in [31; 36] in which the k_{\perp} -factorization framework is employed and the initial condition of the rcBK equation is fixed. The LDMEs are extracted from Tevatron data of prompt J/ψ production at high P_{\perp} . In Fig. 4, the results of the NRQCD in the usual collinear factorization approach at NLO are also shown only in the large P_{\perp} region ($P_{\perp} \gtrsim 5$ GeV, roughly). Regarding J/ψ production in pA collisions at high P_{\perp} , the nuclear PDF is applied to the target nucleus in the NRQCD collinear factorization framework. One finds immediately that the CGC+NRQCD framework succeeds in describing the low P_{\perp} J/ψ production within the uncertainties inherited from the LDMEs, while the NRQCD collinear factorization approach can reproduce the data of J/ψ production at large P_{\perp} both in pp and pA collisions at RHIC and LHC within large kinematical windows.

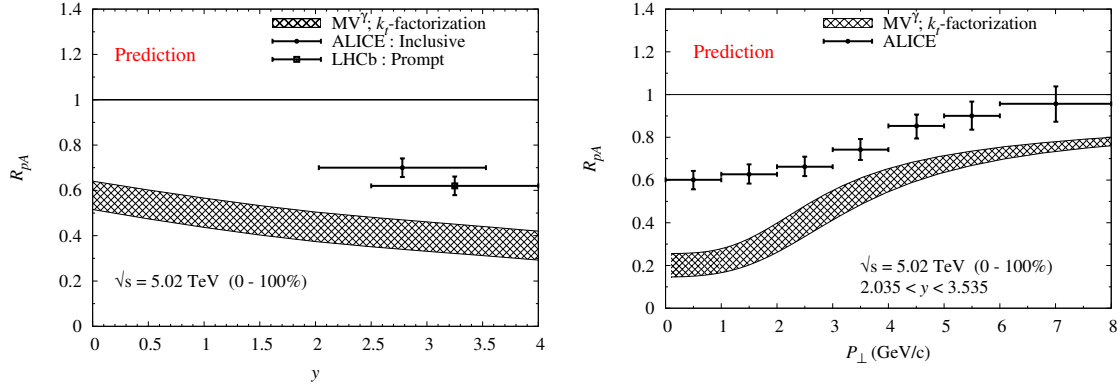


Fig. 5 Early predictions of R_{pA} of J/ψ production at LHC in the CGC+CEM framework [25].

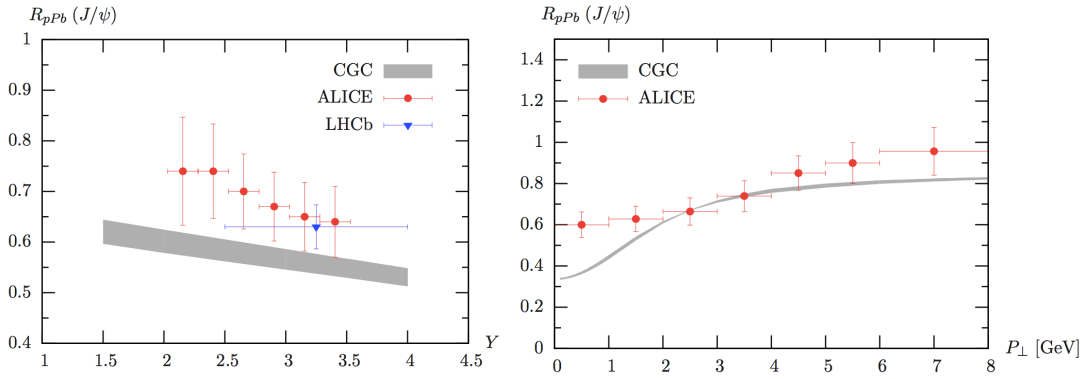


Fig. 6 Improved results of R_{pA} of J/ψ production at LHC in the CGC+CEM framework with the use of Eq. (27). The figures are from [39].

As mentioned in Sec. 5, it is expected that the color singlet direct J/ψ production can be enhanced in pA collision compared to pp collision. In fact, Refs. [31; 36] reported that the contribution of the color singlet direct J/ψ production is about 10% of the total cross section in pp collision at most and 15%-20% at low P_{\perp} in pA collision. Therefore, although the contribution of the color singlet channel is slightly enhanced in pA collision than in pp collision, the CGC+CSM framework is not important.

6.2 Nuclear suppression in minimum bias events

Quarkonium production in the CGC framework contain the large uncertainties in association with the input parameters, the initial condition of the rcBK equation, and the models of the bound state formation. These large uncertainties should be reduced in nuclear modification factor which is defined as

$$R_{pA} = \frac{1}{A} \frac{d^3\sigma_{pA}/d^2P_{\perp}dy}{d^3\sigma_{pp}/d^2P_{\perp}dy}. \quad (32)$$

The R_{pA} of J/ψ production in pA collisions at LHC in the CGC+CEM framework, which was predicted in [25], is indeed far off the LHC data at forward rapidity as shown in Fig. 5. In [25], Eq. (26) with $c = 1$ is employed as the rcBK initial condition for minimum bias events in pA collisions. However, this model is too simplified and then some information of the nuclear profile can be required to understand the strong suppression of the R_{pA} in the CGC framework at LHC.

The nuclear density effect on the R_{pA} with the use of optical Glauber model are examined accordingly in Ref. [39] in the Hybrid formula with the CEM. The improved results of the R_{pA} in the CGC+CEM framework shown in Fig. 6 approach the LHC data. Interestingly, by using Eq. (26) with $c = 0.5$ as the initial condition

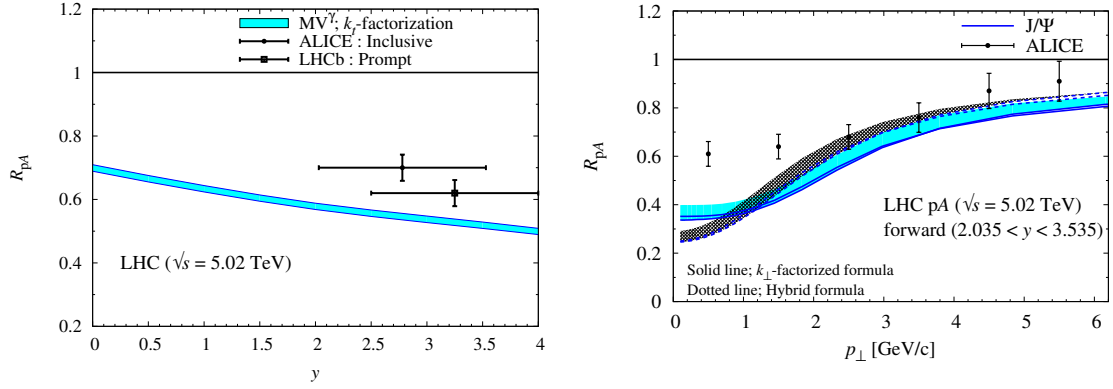


Fig. 7 Improved results of R_{pA} of J/ψ production at LHC in the CGC+CEM framework by employing Eq. (26) with $c = 0.5$ [37].

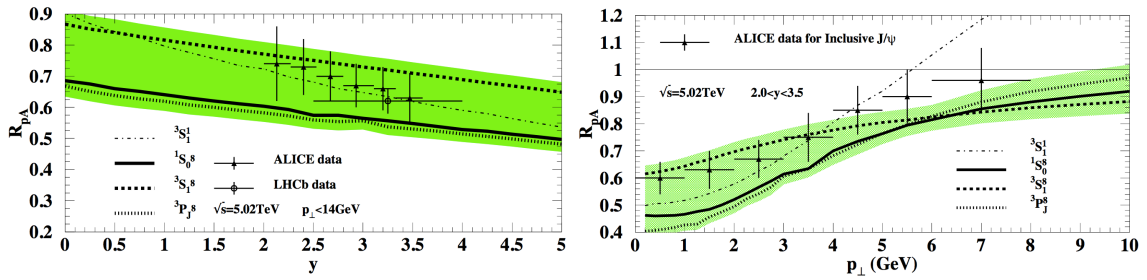


Fig. 8 R_{pA} of forward J/ψ production at LHC in the CGC+NRQCD framework. The figures are taken from Ref. [36].

of the rcBK equation¹¹, the similar suppressions of the R_{pA} shown in Fig. 7 are obtained in the CGC+CEM framework [37].

Fig. 8 shows the R_{pA} computed in the CGC+NRQCD framework [36] in which a similar small saturation scale is used in the rcBK equation for nucleus¹². The CGC+NRQCD involves the large uncertainties associated with the color octet LDMEs. Then, it is hard to determine the most dominant channel for J/ψ production. Nevertheless, the nuclear suppressions in the CGC+NRQCD framework are in agreement with data within the large uncertainties.

6.3 Event activity dependence

In addition to minimum bias events, event activity dependence (or centrality dependence) of quarkonium production in pA collisions can provide unique observables to investigate further the gluon saturation dynamics in the target nucleus. The nuclear modification factor in each event activity in pA collision is defined as

$$Q_{pA} = \frac{1}{A\langle T_A \rangle} \frac{d^3 N_{pA}/d^2 P_{\perp} dy}{d^3 \sigma_{pp}/d^2 P_{\perp} dy} \quad (33)$$

where $d^3 N_{pA}/d^2 P_{\perp} dy$ is the invariant yield in pA collisions and $\langle T_A \rangle$ is related to the number of binary collision N_{coll} , namely the centrality classes [52]. It is naively anticipated that the nuclear suppression due to the gluon saturation effect should be more pronounced in most central collision (large N_{coll}) rather than peripheral collisions or minimum bias event because the large saturation scale is involved in the central collision.

Fig. 9 (left) shows the Q_{pA} of forward J/ψ production at LHC as a function of N_{coll} by integrating over P_{\perp} . The theoretical results are computed in Ref. [40] by using the Hybrid formula with the CEM. To evaluate N_{coll} , different models including the optical Glauber model (27) have been used. As indicated in [40], the

¹¹ $Q_{s0,A}^2 = 3Q_{s0}^2$ is used for numerical calculations in [37].

¹² In Ref. [36], the MV model is used as the initial condition of the rcBK equation. Consequently, the choice of $Q_{s0,A}^2 = 2Q_{s0}^2$ leads to Fig. 8.

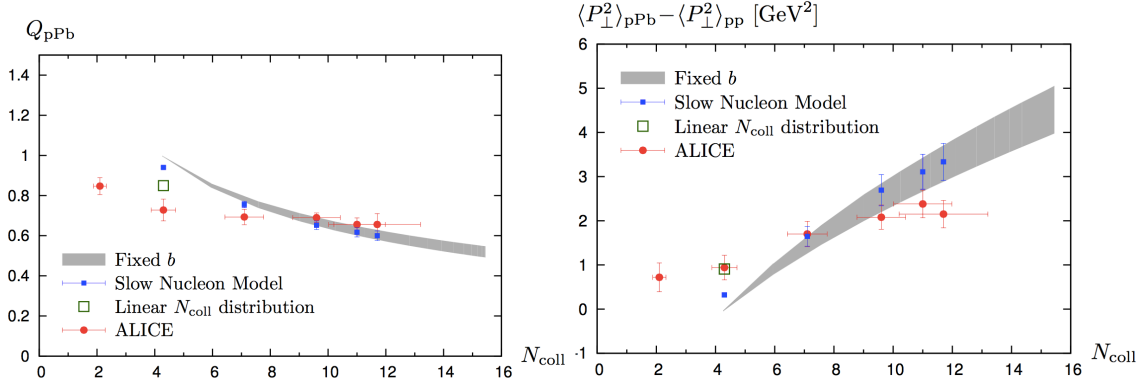


Fig. 9 Event activity dependence of Q_{pA} (left) and $\Delta\langle P_{\perp}^2 \rangle_{pA}$ (left) for forward J/ψ production at LHC. Figures are taken from Ref. [40].

theoretical results strongly depend on the distribution of N_{coll} in pA collision and further study in this respect is required to reproduce data quantitatively.

Fig. 9 (right) shows N_{coll} dependence of the P_{\perp} broadening of forward J/ψ production at LHC, defined as $\Delta\langle P_{\perp}^2 \rangle_{pA} = \langle P_{\perp}^2 \rangle_{pA} - \langle P_{\perp}^2 \rangle_{pp}$. One finds that the $\Delta\langle P_{\perp}^2 \rangle_{pA}$ depends on the nuclear density as well.

7 Sudakov implementation in the Small- x formalism

As seen in the previous sections, the CGC+CEM/NRQCD approaches reproduce the P_{\perp} dependence of forward J/ψ production both in pp and pA collisions at LHC within the large uncertainties of normalization. However, the CGC framework can not describe P_{\perp} dependence of Υ production at LHC [25; 39]. Indeed, the LHCb data [53] shows that the mean P_{\perp} of Υ in pp collisions is larger than that of J/ψ [54] for a wide range of rapidity windows. In principle, regarding Υ production, although the mass scale is different from J/ψ , one expects that the P_{\perp} broadening of Υ should be similar or slightly smaller than the one for J/ψ due to the saturation effects with similar kinematics and physical input parameters between Υ and J/ψ . The difference of mass scale between J/ψ and Υ is roughly a factor of 3 at most. This implies that both J/ψ and Υ can probe the dense gluons at $Q_s \sim 1$ GeV in the target proton.

A point is two kinds of hard scales for heavy quarkonium production. The first hard scale is mass of heavy quarkonium M . The second one is transverse momentum of quarkonium P_{\perp} . Then, in the high scattering energy region, one finds the ordering $s \gg M^2 \gg P_{\perp}^2 \sim Q_s^2 \gg \Lambda_{\text{QCD}}^2$. The order $s \gg P_{\perp}^2$ can bring a large correction as $\frac{\alpha_s N_c}{2\pi^2} \ln \frac{1}{x}$ which can be resummed by means of the BK equation, while the order $M^2 \gg P_{\perp}^2$ can yield another large correction as $\frac{\alpha_s N_c}{2\pi} \ln^2 \frac{M^2}{P_{\perp}^2}$ which is exactly Sudakov double logarithmic correction [17; 55] and can be resummed in so-called Collins-Soper-Sterman (CSS) formalism [56]. The CSS formalism is a unique formalism to enable us to implement Sudakov factor in coordinate space. The Sudakov factor concerned with soft gluons emission has been missing in all of the CGC calculations for quarkonium production. However, as long as we restrict our attention into low- P_{\perp} heavy quarkonium production, it is essential to take into consideration both the JIMWLK/BK evolution and the CSS evolution simultaneously in the Small- x formalism.

Let us review the results of Υ production in pp collision in the CGC+CEM framework with the Sudakov factor implemented in Ref. [57]. Essentially, in the CGC framework, mean P_{\perp} of quarkonium can be supplied by kicks from the dense gluons in target hadron/nucleus. However, by taking into account the Sudakov factor, the differential cross section for forward $q\bar{q}$ production in pp collisions, which was used in the CGC+CEM framework, can be cast into

$$\frac{d\sigma_{q\bar{q}}}{d^2q_{\perp} d^2p_{\perp} dy_q dy_p} = \frac{\alpha_s N_c S_{\perp}}{64\pi^2 C_F} \int d^2l_{\perp} d^2k_{\perp} \Xi_{\text{coll}}(k_{2\perp}, k_{\perp} - z l_{\perp}) F_{\text{TMD}}(l_{\perp}) F_{Y_g}(k_{\perp}) F_{Y_g}(k_{2\perp} - k_{\perp} + l_{\perp}) \quad (34)$$

where new transverse momentum dependent (TMD) gluon distribution function is defined as

$$F_{\text{TMD}}(M, l_{\perp}) = \int \frac{d^2b_{\perp}}{(2\pi)^2} e^{-ib_{\perp} \cdot l_{\perp}} e^{-S_{\text{Sud}}(M, b_{\perp})} x_p G\left(x_p, \mu = \frac{c_0}{b_{\perp}}\right). \quad (35)$$

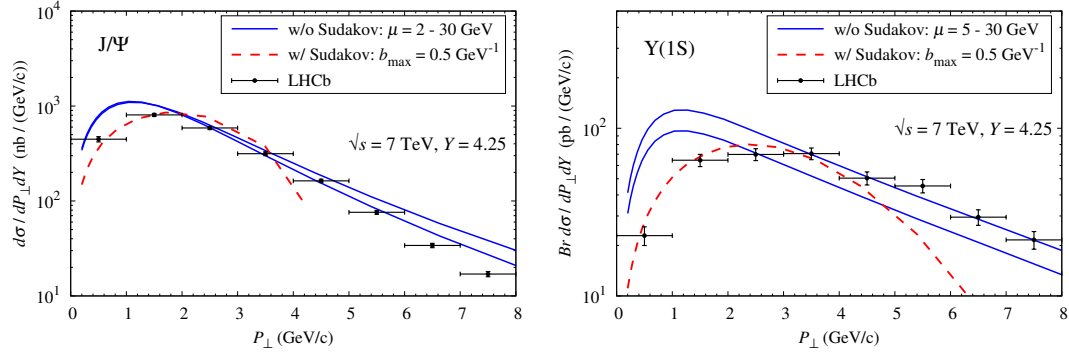


Fig. 10 Double differential cross sections of J/ψ and Y as a function of P_\perp for $Y = 4.25$ in pp collisions at $\sqrt{s} = 7$ TeV. The results are obtained by using Eq. (34) with the CEM [57].

$x_p G$ is the collinear gluon distribution function applied on the projectile proton. Y_g is the rapidity gap between the $q\bar{q}$ and the target proton. In the CSS formalism, the Sudakov factor is separated from the perturbative part and the nonperturbative part as $S_{\text{Sud}}(M, b) = S_{\text{perp}}(M, b_\star) + S_{\text{NP}}(M, b)$ with b_\star -prescription: $b_\star = b/\sqrt{1 + (b/b_{\text{max}})^2}$. The perturbative part for $b_\star \sim b \ll b_{\text{max}}$ is given by

$$S_{\text{perp}}(M, b) = \int_{c_0/b^2}^{M^2} \frac{d\mu^2}{\mu^2} \left[A \ln \left(\frac{M^2}{\mu^2} \right) + B \right] \quad (36)$$

where the coefficient functions A and B have been calculated perturbatively $A = \sum_{i=1} A^{(i)} \left(\frac{\alpha_s}{\pi} \right)^i$ and $B = \sum_{i=1} B^{(i)} \left(\frac{\alpha_s}{\pi} \right)^i$ respectively. For the one loop correction, they are given by $A^{(1)} = C_A$ and $B^{(1)} = -(b_0 + \frac{1}{2} \delta_{8c}) N_c$ where $b_0 = \left(\frac{11}{6} N_c - \frac{n_f}{3} \right) \frac{1}{N_c}$. As for $B^{(1)}$, the factor δ_{8c} is significant only in the production of a color octet $q\bar{q}$.

The non-perturbative part for $b > b_{\text{max}}$ can be determined by data fitting as performed in Ref. [55] with use the following function

$$S_{\text{NP}}(M, b) = \exp \left[\frac{b^2}{2} \left(-g_1 - g_2 \ln \left(\frac{M}{2Q_0} \right) - g_1 g_3 \ln(100 x_p x_g) \right) \right] \quad (37)$$

where the fitting parameters $g_1, g_2, g_1 g_3, Q_0, b_{\text{max}}$ are found in Ref. [55].

FIG. 10 shows the results for J/ψ and Y productions in pp collisions at $\sqrt{s} = 7$ TeV. As shown in Refs. [25; 39], the Y production with only the small- x resummation does not yield enough transverse momentum broadening as compared to data. Eq. (34) with the use of the CEM reproduces the data points very well due to the gluon cascade characterized by the Sudakov factor. Of particular importance is that the Sudakov factor in association with large M gives additional strong broadening of the p_\perp distributions for Y production. Therefore, the Sudakov factor is indispensable in order to consistently describe both J/ψ and Y productions in the Small- x formalism.

A comment is noted here: The factorization scale μ is normally arbitrary at LO. At NLO, one can choose μ to minimize K -factor. Indeed, as shown in Fig. 10, μ is chosen between 2 or 5 GeV to 30 GeV in the LO CGC calculations without the Sudakov factor. On the other hand, in the CSS formalism, one can choose $\mu = c_0/b_\perp$ in coordinate space. Then, there is no uncertainty associated with the choice of μ in Fig. 10.

In addition, one must keep in mind that the so-called Y -term is missing in this calculation [58]. Necessarily, F_{TMD} goes to negative at $P_\perp \gtrsim M$ in which the CSS resummation is broken down. Indeed, one finds in Fig. 10 that the P_\perp spectrums of J/ψ and Y with the Sudakov factor drop rapidly at large P_\perp . The Y -term is required to connect the CSS formalism to fixed order CGC calculation which is responsible for the large P_\perp region of the spectrums, although one should switch the CGC framework to the collinear factorization framework at large P_\perp .

8 Summary

In this paper, we have reviewed quarkonium production in pp and pA collisions at the RHIC and the LHC energies in the Small- x formalism. The CGC framework provides a systematic description of heavy quark pair production in dilute-dense system. However, the CGC framework has been confronted with some issues to describe differential cross section of quarkonium production quantitatively. As discussed in Sec. 4, the CGC framework contains the uncertainties concerning the initial condition of the rcBK equation for nucleus and the extrapolation of the dipole amplitude at large- x . Furthermore, the CGC+CEM/NRQCD approaches involve the uncertainties of the input parameters, such as quark mass scale and the LDMEs.

Nevertheless, as shown in Sec. 6, the nuclear modification factors for minimum bias events and several centrality classes in pA collision can play a crucial role to constrain the model of the initial condition of the rcBK equation for nucleus, since the large systematic uncertainties should be reduced by definition. This constrain can lead to understanding of the onset of the gluon saturation phenomenologically.

The Sudakov effect on top of the saturation effect in the small- x formalism, which is discussed in Sec. 7, could change the nuclear modification factor quantitatively, although full NLO calculations for heavy quark pair production in the Small- x formalism are not completed yet. In this respect, further theoretical efforts are required.

Acknowledgements This work is supported by the National Science Foundation of China (NSFC) under Grant No. 11575070. I would like to thank F. Arleo, B. Ducloué, J.-P. Lansberg, T. Lappi, H. Fujii, Y.-Q. Ma, R. Venugopalan, B.-W. Xiao, F. Yuan for interesting discussions and comments.

References

1. L. V. Gribov, E. M. Levin and M. G. Ryskin, Phys. Rept. **100**, 1 (1983).
2. A. H. Mueller and J. w. Qiu, Nucl. Phys. B **268**, 427 (1986).
3. A. H. Mueller, hep-ph/0111244.
4. A. Andronic *et al.*, Eur. Phys. J. C **76**, no. 3, 107 (2016) [arXiv:1506.03981 [nucl-ex]].
5. H. Weigert, Prog. Part. Nucl. Phys. **55**, 461 (2005) [hep-ph/0501087].
6. F. Gelis, E. Iancu, J. Jalilian-Marian and R. Venugopalan, Ann. Rev. Nucl. Part. Sci. **60**, 463 (2010) [arXiv:1002.0333 [hep-ph]].
7. Y. V. Kovchegov and E. Levin, “Quantum chromodynamics at high energy,” (2012), Cambridge University Press.
8. J. Jalilian-Marian, A. Kovner, A. Leonidov and H. Weigert, Nucl. Phys. B **504** (1997) 415 [arXiv:hep-ph/9701284].
9. J. Jalilian-Marian, A. Kovner, A. Leonidov and H. Weigert, Phys. Rev. D **59**, 014014 (1998) [hep-ph/9706377].
10. E. Iancu, A. Leonidov and L. D. McLerran, Phys. Lett. B **510**, 133 (2001) [hep-ph/0102009].
11. E. Iancu, A. Leonidov and L. D. McLerran, Nucl. Phys. A **692**, 583 (2001) [hep-ph/0011241].
12. H. Weigert, Nucl. Phys. A **703**, 823 (2002) [hep-ph/0004044].
13. I. Balitsky, Nucl. Phys. B **463**, 99 (1996) [hep-ph/9509348].
14. Y. V. Kovchegov, Phys. Rev. D **54**, 5463 (1996) [hep-ph/9605446].
15. N. Brambilla *et al.*, Eur. Phys. J. C **71**, 1534 (2011) [arXiv:1010.5827 [hep-ph]].
16. D. Kharzeev and K. Tuchin, Nucl. Phys. A **770**, 40 (2006) [hep-ph/0510358].
17. J. W. Qiu, P. Sun, B. W. Xiao and F. Yuan, Phys. Rev. D **89**, no. 3, 034007 (2014) [arXiv:1310.2230 [hep-ph]].
18. G. T. Bodwin, E. Braaten and J. Lee, Phys. Rev. D **72**, 014004 (2005) [hep-ph/0504014].
19. J. P. Blaizot, F. Gelis and R. Venugopalan, Nucl. Phys. A **743**, 13 (2004) [hep-ph/0402256].
20. J. P. Blaizot, F. Gelis and R. Venugopalan, Nucl. Phys. A **743**, 57 (2004) [hep-ph/0402257].
21. K. Tuchin, Phys. Lett. B **593**, 66 (2004) doi:10.1016/j.physletb.2004.04.057 [hep-ph/0401022].
22. Y. V. Kovchegov and K. Tuchin, Phys. Rev. D **74**, 054014 (2006) [hep-ph/0603055].
23. H. Fujii, F. Gelis and R. Venugopalan, Nucl. Phys. A **780**, 146 (2006) [hep-ph/0603099].
24. H. Fujii, F. Gelis and R. Venugopalan, Phys. Rev. Lett. **95**, 162002 (2005) [hep-ph/0504047].
25. H. Fujii and K. Watanabe, Nucl. Phys. A **915**, 1 (2013) [arXiv:1304.2221 [hep-ph]].
26. Z. B. Kang, Y. Q. Ma and R. Venugopalan, JHEP **1401**, 056 (2014) [arXiv:1309.7337 [hep-ph]].
27. K. J. Golec-Biernat and M. Wusthoff, Phys. Rev. D **59**, 014017 (1998) [hep-ph/9807513].
28. I. Balitsky, Phys. Rev. D **75**, 014001 (2007) [hep-ph/0609105].
29. J. L. Albacete, A. Dumitru, H. Fujii and Y. Nara, Nucl. Phys. A **897**, 1 (2013) [arXiv:1209.2001 [hep-ph]].
30. J. L. Albacete and C. Marquet, Prog. Part. Nucl. Phys. **76**, 1 (2014) [arXiv:1401.4866 [hep-ph]].
31. Y. Q. Ma and R. Venugopalan, Phys. Rev. Lett. **113**, no. 19, 192301 (2014) [arXiv:1408.4075 [hep-ph]].
32. J. L. Albacete, N. Armesto, J. G. Milhano and C. A. Salgado, Phys. Rev. D **80**, 034031 (2009) [arXiv:0902.1112 [hep-ph]].
33. J. L. Albacete, N. Armesto, J. G. Milhano, P. Quiroga-Arias and C. A. Salgado, Eur. Phys. J. C **71**, 1705 (2011) [arXiv:1012.4408 [hep-ph]].
34. T. Lappi and H. Mäntysaari, Phys. Rev. D **88**, 114020 (2013) [arXiv:1309.6963 [hep-ph]].
35. L. D. McLerran and R. Venugopalan, Phys. Rev. D **49**, 2233 (1994) [hep-ph/9309289], Phys. Rev. D **49**, 3352 (1994) [hep-ph/9311205], Phys. Rev. D **50**, 2225 (1994) [hep-ph/9402335].
36. Y. Q. Ma, R. Venugopalan and H. F. Zhang, Phys. Rev. D **92**, 071901 (2015) [arXiv:1503.07772 [hep-ph]].

-
37. H. Fujii and K. Watanabe, Nucl. Phys. A **951**, 45 (2016) [arXiv:1511.07698 [hep-ph]].
 38. K. Dusling, F. Gelis, T. Lappi and R. Venugopalan, Nucl. Phys. A **836**, 159 (2010) [arXiv:0911.2720 [hep-ph]].
 39. B. Ducloué, T. Lappi and H. Mäntysaari, Phys. Rev. D **91**, no. 11, 114005 (2015) [arXiv:1503.02789 [hep-ph]].
 40. B. Ducloué, T. Lappi and H. Mäntysaari, Phys. Rev. D **94**, no. 7, 074031 (2016) [arXiv:1605.05680 [hep-ph]].
 41. F. Dominguez, C. Marquet, B. W. Xiao and F. Yuan, Phys. Rev. D **83**, 105005 (2011) [arXiv:1101.0715 [hep-ph]].
 42. Y. Q. Ma, K. Wang and K. T. Chao, Phys. Rev. Lett. **106**, 042002 (2011) doi:10.1103/PhysRevLett.106.042002 [arXiv:1009.3655 [hep-ph]].
 43. M. Butenschoen and B. A. Kniehl, Phys. Rev. Lett. **106**, 022003 (2011) doi:10.1103/PhysRevLett.106.022003 [arXiv:1009.5662 [hep-ph]].
 44. K. T. Chao, Y. Q. Ma, H. S. Shao, K. Wang and Y. J. Zhang, Phys. Rev. Lett. **108**, 242004 (2012) doi:10.1103/PhysRevLett.108.242004 [arXiv:1201.2675 [hep-ph]].
 45. B. Kopeliovich, A. Tarasov and J. Hufner, Nucl. Phys. A **696**, 669 (2001) [hep-ph/0104256].
 46. B. Z. Kopeliovich, I. K. Potashnikova, H. J. Pirner and I. Schmidt, Phys. Rev. C **83**, 014912 (2011) [arXiv:1008.4272 [hep-ph]].
 47. B. Z. Kopeliovich, I. K. Potashnikova and I. Schmidt, Nucl. Phys. A **864**, 203 (2011) [arXiv:1012.5648 [hep-ph]].
 48. F. Dominguez, D. E. Kharzeev, E. M. Levin, A. H. Mueller and K. Tuchin, Phys. Lett. B **710**, 182 (2012) [arXiv:1109.1250 [hep-ph]].
 49. D. E. Kharzeev, E. M. Levin and K. Tuchin, Nucl. Phys. A **924**, 47 (2014) [arXiv:1205.1554 [hep-ph]].
 50. D. Kharzeev, E. Levin, M. Nardi and K. Tuchin, Phys. Rev. Lett. **102**, 152301 (2009) [arXiv:0808.2954 [hep-ph]].
 51. J. Pumplin, D. R. Stump, J. Huston, H. L. Lai, P. M. Nadolsky and W. K. Tung, JHEP **0207**, 012 (2002) [hep-ph/0201195].
 52. J. Adam *et al.* [ALICE Collaboration], JHEP **1511**, 127 (2015) [arXiv:1506.08808 [nucl-ex]].
 53. R. Aaij *et al.* [LHCb Collaboration], Eur. Phys. J. C **72**, 2025 (2012) [arXiv:1202.6579 [hep-ex]].
 54. R. Aaij *et al.* [LHCb Collaboration], Eur. Phys. J. C **71**, 1645 (2011) [arXiv:1103.0423 [hep-ex]].
 55. P. Sun, C.-P. Yuan and F. Yuan, Phys. Rev. D **88**, 054008 (2013) doi:10.1103/PhysRevD.88.054008 [arXiv:1210.3432 [hep-ph]].
 56. J. C. Collins, D. E. Soper and G. F. Sterman, Nucl. Phys. B **250**, 199 (1985).
 57. K. Watanabe and B. W. Xiao, Phys. Rev. D **92**, no. 11, 111502 (2015) [arXiv:1507.06564 [hep-ph]].
 58. M. Boglione, J. O. Gonzalez Hernandez, S. Melis and A. Prokudin, JHEP **1502**, 095 (2015) [arXiv:1412.1383 [hep-ph]].